Direct observation of spontaneous strain variation and domain evolution in the phase transition of NdP_5O_{14}

X. R. Huang, S. S. Jiang, Z. W. Hu, X. Y. Xu, and W. Zeng
National Laboratory of Solid State Microstructures, Nanjing University, Nanjing 210008, China

J. H. Jiang
Beijing Synchrotron Radiation Laboratory, Institute of High Energy Physics, Beijing 10039, China

J. Y. Wang
Institute of Crystal Materials, Shandong University, Jinan 250100, China

D. Feng
National Laboratory of Solid State Microstructures, Nanjing University, Nanjing 210008, China
(Received 18 April 1994; revised manuscript received 10 June 1994)

White-beam synchrotron-radiation topography is applied to an investigation of the second-order ferroelastic-paraelastic phase transition in NdP_5O_{14} single crystals. The displacements of images of adjacent domains in the 200 reflection topographs and their variation during the transition are directly observed with a television recording system. The spontaneous deformation, a monoclinic shear strain e_5, is calculated from the image displacements at different temperatures. The temperature dependence of e_5 and the evolution of domains are well consistent with the Landau theory of second-order phase transitions. The transition process is also observed under a polarizing microscope.

I. INTRODUCTION

Ferroelasticity is associated with many kinds of materials including some high-T_c superconductors and it has attracted the investigators' attention for many years.[1-4] It is well known that the domain structure and domain dynamical behaviors can substantially influence the main properties of ferroic crystals. The existence and switching of domains are among the most important characteristics of ferroelastics and related materials. But in experiments there are still fewer direct methods in studying and observing ferroelastic behaviors in crystals compared with ferromagnetics or ferroelectrics. This research work is simulated by new experimental methods of visualization of ferroelastic domain structures and their dynamics.

Synchrotron radiation (SR) is an interdisciplinary tool in scientific research. Using the hard x ray of high intensity, continuous wavelength distribution, and natural collimation, some work has been carried out concerning domain configuration and *in situ* observation of phase transition in ferroic crystals through SR topography.[5-8] In this paper, we use SR transmission topography to study the ferroelastic-paraelastic phase transition of neodymium pentaphosphate NdP_5O_{14} (NPP) crystals. Especially, we report the direct observation of the variation of the spontaneous shear strain in NPP during the phase transition for the first time. In our experiments, the dynamical ferroelastic behaviors and the whole process of the phase transition are also revealed at the same time. Furthermore, this white-beam topographic observation of spontaneous strain and its variation is a simple and convenient technique because there is no need for strict diffraction condition or accurate positioning of the sample, compared with that in γ-ray diffraction,[9] optical reflection,[10] and other methods. In addition to the topographic observation, the results obtained from polarized light are also summarized and discussed.

II. DOMAIN STRUCTURE AND GEOMETRY OF DIFFRACTION

When the transition in NPP takes place from *Pncm* to $P2_1/c$, according to the space-group theory of Guymont[11] and the strain compatibility condition of Sapriel,[12] two different kinds of orientational domains (orientational variants) occur. The domains are ferroelastic twins with two types of permissible twin boundaries parallel to the (001) and (100) planes of the prototype phase, respectively: the former is called "*a*-type twin" and the latter is called "*b*-type twin," as shown in Fig. 1(a).[13] The schematic representations of the twin structures are shown in Fig. 1(b) and 1(c). For the *a*-type twin in Fig. 1(b), there is a rotation of the *c* axis by a small angle δ ($\delta \sim 0.5°$ at room temperature). Thus, the thermal-strain tensor appearing in a free NPP takes the following form:

$$\begin{bmatrix} e_1 & 0 & \frac{1}{2}e_5 \\ 0 & e_2 & 0 \\ \frac{1}{2}e_5 & 0 & e_3 \end{bmatrix} \quad (1)$$

in the frame of reference constituted by the three crystallographic orthorhombic axes where $e_5=\delta$ is the spontaneous shear strain which vanishes by symmetry in the

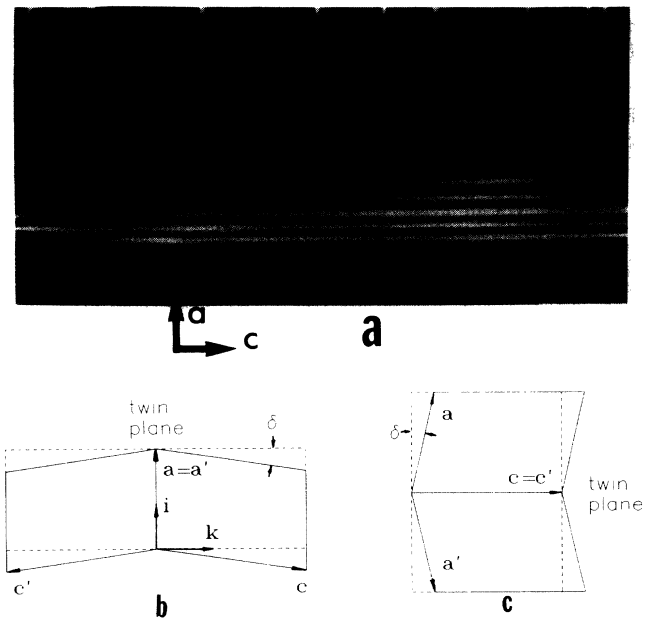

FIG. 1. Twinning in NPP. (a) Optical visualization of a-type twins (vertical domains) and b-type twins (horizontal domains); (b) a-type twin structure; (c) b-type twin structure.

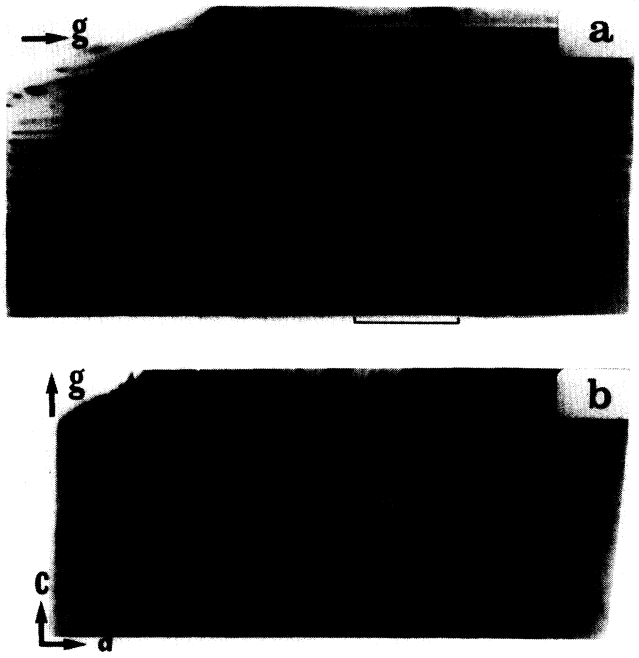

FIG. 2. SR topographs of NPP at room temperature; B, growth sector boundaries. (a) 200 reflection showing displacements of a-type twin images; (b) 001 reflection showing no contrast of twin.

orthorhombic phase. The diagonal terms of matrix (1) represent expansions along the three orthorhombic axes of the prototype phase and take the same value for the two kinds of domains. Generally, the shear strain e_5 is chosen as the order parameter which takes $+e_5$ and $-e_5$ for the two kinds of domains of NPP, respectively.

In a twinned NPP, the small shear strain produces a small discontinuity in orientation between two neighboring domains. Consider an a-type twin boundary between two domains, 1 and 2, as indicated in Fig. 1(b). The lattice planes (hkl) in domain 1 continue across the boundary into domain 2 as $(h'k'l')$ only with a slight tilt, where

$$h'=h\ ,\quad k'=-k\ ,\quad l'=-l\ . \tag{2}$$

When we take white-beam x-ray topographs of the crystal, the lattice planes (hkl) and $(h'k'l')$ select out of the continuous spectrum the proper wavelengths to be reflected according to the well-known Bragg's law

$$2d_{hkl}\sin\theta=n\lambda\ , \tag{3a}$$

$$2d_{h'k'l'}\sin\theta'=n\lambda'\ , \tag{3b}$$

where d_{hkl} and $d_{h'k'l'}$ are the inteplanar spacing of (hkl) and $(h'k'l')$ planes with $d_{hkl}=d_{h'k'l'}$, θ and θ' are halves of scattering angles, and n is an integer. Usually an angular divergence between the two reflected beams arises from the slight difference between θ and θ', which results in displacements of domain images in topographs. For instance, in the 200 reflection of Fig. 2(a), the separation and overlapping of the horizontal a-type twin images are clearly revealed. However, there is no contrast of a-type twins in any $00l$ reflection topograph [Fig. 2(b)] since the $(00l)$ lattice planes in adjacent domains are exactly parallel. The intense contrast marked as B in Figs. 2(a) and 2(b) are contrast of growth sector boundaries.

If we regard the top section of Fig. 2(a) as a single domain 1 and the bottom as a domain 2, then a schematic interpretation of Fig. 2(a) is obtained as Fig. 3 with the images of these two domains moving away from each other.

Consider, in particular, two diffracted rays emanating from adjacent points very close to O on the boundary with each ray undergoing diffraction from its respective domain. Let $\mathbf{n}_{hkl}$ and $\mathbf{n}_{h'k'l'}$ be the normals of the adjacent lattice planes with a slight discontinuity on the boundary, respectively, and $\mathbf{n}_{in}=\mathbf{k}_{in}/|\mathbf{k}_{in}|$ be a unit vector along the wave vector $\mathbf{k}_{in}$ of the incident beam, then for the diffraction of domain 1, the Bragg angle θ

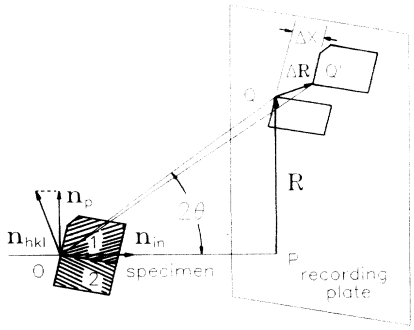

FIG. 3. Geometry of diffraction and interpretation of image displacement in Fig. 2(a), $\Delta\mathbf{R}$ is the relative displacement of the images of domain 1 and 2.

($0<\theta<\pi/4$ for transmission diffraction) takes the following form according to Fig. 3:

$$\cos(\theta+\pi/2)=-\sin\theta=\mathbf{n}_{\text{in}}\cdot\mathbf{n}_{hkl} , \tag{4}$$

where $\mathbf{n}_{hkl}=(h\mathbf{a}^*+k\mathbf{b}^*+l\mathbf{c}^*)/|h\mathbf{a}^*+k\mathbf{b}^*+l\mathbf{c}^*|$ and $\mathbf{a}^*$, $\mathbf{b}^*$, and $\mathbf{c}^*$ are the reciprocal-lattice vectors of domain 1.

In the experiment, $\mathbf{n}_{\text{in}}$ is perpendicular to the recording plate and the distance between the specimen and the plate is D. If the transmitted image of O on the plate is P and the hkl reflection image of O is Q, then we obtain

$$\overline{PQ}=D\tan2\theta . \tag{5}$$

The vector $\mathbf{R}$ from P to Q is parallel to the perpendicular component $\mathbf{n}_p$ of $\mathbf{n}_{hkl}$ with $\mathbf{n}_p\perp\mathbf{n}_{\text{in}}$, where

$$\mathbf{n}_p=\mathbf{n}_{hkl}-(\mathbf{n}_{hkl}\cdot\mathbf{n}_{\text{in}})\mathbf{n}_{\text{in}} . \tag{6}$$

Thus, the vector $\mathbf{R}$ can be written as

$$\mathbf{R}=D\tan2\theta\frac{\mathbf{n}_p}{|\mathbf{n}_p|} . \tag{7}$$

In a similar way, the vector $\mathbf{R}'$ corresponding to the diffraction of domain 2 is

$$\mathbf{R}'=D\tan2\theta'\frac{\mathbf{n}'_p}{|\mathbf{n}'_p|} , \tag{8}$$

where $\mathbf{n}'_p=\mathbf{n}_{h'k'l'}-(\mathbf{n}_{\text{in}}\cdot\mathbf{n}_{h'k'l'})\mathbf{n}_{\text{in}}$, $\mathbf{n}_{h'k'l'}=h'\mathbf{a}'^*+k'\mathbf{b}'^*+l'\mathbf{c}'^*$, and $\theta'=\sin^{-1}(\mathbf{n}_{\text{in}}\cdot\mathbf{n}_{h'k'l'})$, $\mathbf{a}'^*$, $\mathbf{b}'^*$, and $\mathbf{c}'^*$ are the reciprocal vectors of domain 2. Eventually the image displacement of any hkl reflection is expressed as

$$\Delta\mathbf{R}=\mathbf{R}'-\mathbf{R} . \tag{9}$$

Usually $\Delta\mathbf{R}$ is dependent on the values of $\mathbf{a}$, $\mathbf{b}$, and $\mathbf{c}$. In order to eliminate the influence of the expansions of $\mathbf{a}$, $\mathbf{b}$, and $\mathbf{c}$ during the phase transition, we choose the 200 reflection because the normals of (200) planes in both domains are independent of $\mathbf{a}$, $\mathbf{b}$, and $\mathbf{c}$ and can be expressed as

$$\mathbf{n}_{200}=\cos\delta\hat{i}+\sin\delta\hat{k},\quad \mathbf{n}'_{200}=\cos\delta\hat{i}-\sin\delta\hat{k} . \tag{10}$$

Then

$$\begin{aligned}\sin\theta&=-\mathbf{n}_{\text{in}}\cdot\mathbf{n}_{hkl}=-n_1\cos\delta-n_3\sin\delta ,\\ \sin\theta'&=-n_1\cos\delta+n_3\sin\delta ,\end{aligned} \tag{11}$$

where n_1,n_2,n_3 are the direction cosines of $\mathbf{n}_{\text{in}}$ in the orthogonal system. From Eqs. (4)–(11), we obtain strictly

$$\begin{aligned}\Delta R=2D\Bigg\{&\left[\cos\delta\left[\frac{x_2}{1-2x_2^2}-\frac{x_1}{1-2x_1^2}\right]+n_1\left[\frac{x_2^2}{1-2x_2^2}-\frac{x_1^2}{1-2x_1^2}\right]\right]\hat{i}+n_2\left[\frac{x_2^2}{1-2x_2^2}-\frac{x_1^2}{1-2x_1^2}\right]\hat{j}\\&-\left[\sin\delta\left[\frac{x_2}{1-2x_2^2}+\frac{x_1}{1-2x_1^2}\right]-n_3\left[\frac{x_2^2}{1-2x_2^2}-\frac{x_1^2}{1-2x_1^2}\right]\right]\hat{k}\Bigg\} ,\end{aligned} \tag{12}$$

where $x_1=\sin\theta$ and $x_2=\sin\theta'$. For general cases, it is easy to measure the displacements along the direction of the twin boundaries in the topographs. As in Fig. 2(a), the a-type boundaries images are along the projection of the crystallographic $\mathbf{a}$ axis on the recording plate. If $\mathbf{n}_a$ is the unit vector along this projection, like Eq. (6), we get

$$\begin{aligned}\mathbf{n}_a&=\frac{\hat{i}-(\hat{i}\cdot\mathbf{n}_{\text{in}})\mathbf{n}_{\text{in}}}{|\hat{i}-(\hat{i}\cdot\mathbf{n}_{\text{in}})\mathbf{n}_{\text{in}}|}\\&=\frac{1}{\sqrt{1-n_1^2}}[(1-n_1^2)\hat{i}-n_1n_2\hat{j}-n_1n_3\hat{k}] .\end{aligned} \tag{13}$$

Then the image displacement along the horizontal direction in Fig. 2(a) is given by

$$\begin{aligned}\Delta X&=\Delta\mathbf{R}\cdot\mathbf{n}_a\\&=\frac{2D}{\sqrt{1-n_1^2}}[(1-n_1^2)(\cos\delta S_1+n_1S_2)-n_1n_2^2S_2\\&\quad+n_1n_3\sin\delta S_3-n_1n_3^2S_2] ,\end{aligned} \tag{14}$$

where

$$\begin{aligned}S_1&=\frac{x_2}{1-2x_2^2}-\frac{x_1}{1-2x_1^2} ,\\ S_2&=\frac{x_2^2}{1-2x_2^2}-\frac{x_1^2}{1-2x_1^2} ,\\ S_3&=\frac{x_1}{1-2x_1^2}+\frac{x_2}{1-2x_2^2} .\end{aligned} \tag{15}$$

It can be seen from Eq. (14) that ΔX are only dependent on $\mathbf{n}$ and δ. The diffraction condition for Fig. 2(a) is calculated strictly from the Laue pattern as $\mathbf{n}=-0.0507\hat{i}+0.987\hat{j}+0.150\hat{k}$, $D=115.31$ mm. In this case, the term $2D\sqrt{1-n_1^2}\cos\delta S_1$ is much greater than the other terms at the right side of Eq. (14) and thus ΔX can be approximated as

$$\begin{aligned}\Delta X&\approx2D\sqrt{1-n_1^2}\cos\delta\left[\frac{x_2}{1-2x_2^2}-\frac{x_1}{1-2x_1^2}\right]\\&\approx\frac{\sqrt{1-n_1^2}\,4Dn_3(1+2n_1^2)}{(1-2n_1^2)^2}\delta .\end{aligned} \tag{16}$$

Through this approximation, ΔX is in direct proportion to δ. In this paper, with the measured value of image displacement, we use Eq. (14) to calculate the magnitude of δ strictly. For example, the magnitude of ΔX in Fig. 2(a) is measured as 0.579 mm, and from Eq. (14) we obtain the value of $\delta = 8.378 \times 10^{-3}$ radian or 0.480° at $T = 20.0$ °C.

III. TEMPERATURE DEPENDENCE OF e_5

In order to study the temperature dependence of $e_5 (= \delta)$, *in situ* observation of phase transition was undertaken at the 4W1A beam line of Beijing Synchrotron Radiation Laboratory (BSRL) with the storage ring running at an energy of 2.2 GeV and a beam current of about 50 mA. An environment chamber is used to control the temperature of the specimen which is a *b*-cut slice with thickness of about 200 μm. It is possible to regulate the chamber temperature with a precision of 0.1 °C. A television recording system is used to observe and record the 200 reflection topographs during the phase transition. The diffraction condition is the same as that of Fig. 2.

Figure 4 shows a series of 200 reflection topographs of the NPP specimen taken at different temperatures during the transition. Upon heating, the image displacement of the *a*-type twins along the horizontal direction is observed to decrease and vanish at 144.3 °C, indicating that the spontaneous strain e_5 decreases with temperature increasing and comes to zero at T_c. Figure 4(d) is the picture taken after the transition at $T = 144.4$ ° C, in which there is no twin contrast or image displacement because at this temperature the crystal has the orthorhombic structure and no twins exist in this phase. In the heating process, we observe no abrupt change of the image displacement, which shows that the spontaneous strain e_5 approaching zero in a gradual way. This is a typical characteristic of second-order phase transitions. From the topographs of different temperatures, the magnitudes of image displacements are measured directly and the corresponding spontaneous strains are calculated with Eq. (14) by computer. The temperature dependence of e_5 and the square of e_5 are plotted in Fig. 5, from which we can see that e_5^2 decreases almost linearly with the increase of temperature within the range $T_c - 10\,°\text{C} \le T \le T_c$,

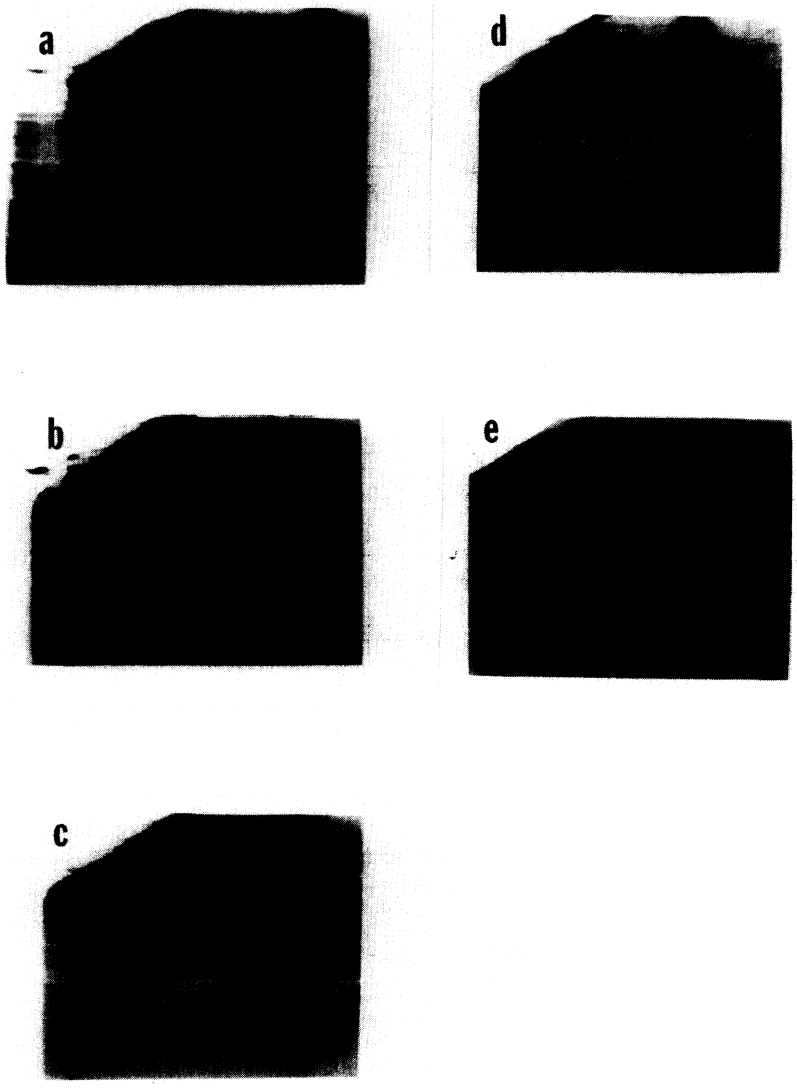

FIG. 4. 200 reflection topographs showing the phase transition of NPP. The temperatures from (a) to (e) are 85.0, 124.0, 140.0, 144.4, and 144.3 °C, respectively. In these figures the decrease of the image displacements is demonstrated. The black contrast to the upper-left section of (e) shows the phase instability.

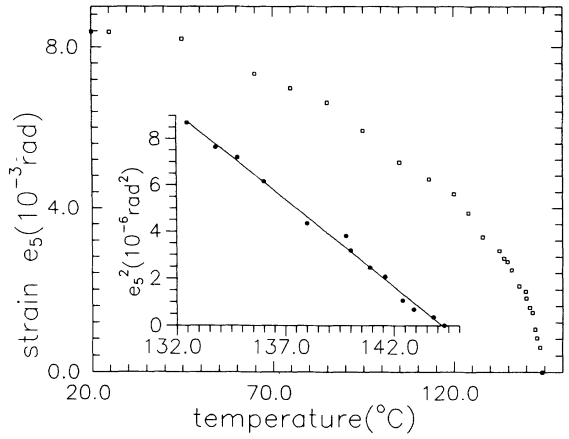

FIG. 5. Variation of spontaneous strain and its square during the phase transition.

showing that e_5 vanishes with a critical exponent $\beta=0.5$, or

$$\eta=e_5=C_0(T_c-T)^{0.5}\ , \tag{17}$$

where $T_c=144.3\,^{\circ}\mathrm{C}$ and C_0 is a constant. These results are expected by the classical Landau theory of second-order phase transition, which is similar to that of LaP_5O_{14}.[9] Moreover, no sharp phase transition front (ferroelastic-paraelastic interface) is observed during the transition. Upon cooling, most of the domains are reintroduced at T slightly below T_c and no thermal hysteresis greater than 0.1 °C is observed. However, it is interesting that when the temperature is indicated as T_c, we find that the contrast of the upper-left section of the specimen varies between Figs. 4(e) and 4(d) for several times, while the contrast of other section remains unchanged. This phenomenon indicates that, due to a slight temperature instability or gradient, the temperature of the upper-left section fluctuates between above and below T_c, which results in the alternation between the paraelastic and ferroelastic states in this region. The instability is believed to be smaller than 0.05 °C, which further proves that if thermal hysteresis exists during the transition, it should be smaller than 0.05 °C.

IV. DOMAIN EVOLUTION IN THE PHASE TRANSITION

According to Landau theory, the free energy of the second-order phase transition is

$$F=\tfrac{1}{2}A_0(T-T_c)\eta^2+\tfrac{1}{4}B_0\eta^4\ , \tag{18}$$

where A_0 and B_0 were weakly temperature independent constant with $A_0,B_0>0$. By minimizing F two different values of the order parameter can be obtained at equilibrium as

$$\eta=\pm\eta_0=\pm\left[\frac{A_0(T_c-T)}{B_0}\right]^{1/2}\sim(T_c-T)^{1/2}\ . \tag{19}$$

In a free NPP, $+\eta_0$ and $-\eta_0$ correspond to the two ferroelastic domains. In Sec. III, we demonstrate that $\eta=e_5$ decreases with the increase of temperature from experiments, which is in good agreement with this theory. When a domain reverses from $+\eta_0$ to $-\eta_0$, it must surmount a potential barrier

$$\Delta F=\frac{A_0^2(T_c-T)^2}{4B_0}\sim(T_c-T)^2\ . \tag{20}$$

ΔF decreases with the increasing temperature, and it can be expected that more twins exist in NPP at high temperature than that at low temperature. This is proved both in topographic and optical observation. In Fig. 2(a), only a few a-type twins exist in the sample when it is at room temperature, but at $T=85.0\,^{\circ}\mathrm{C}$ in Fig. 4(a), many new domains appear. Upon further raising the temperature, the whole crystal is divided into numerous microdomains and we can only see two overlapped images of the whole specimen, which are produced by the alternating thin planes of the two different domains.

The evolution of domains in NPP is also observed with a polarizing microscope (PM) also equipped with a heat stage. The micrographs in Fig. 6 are taken from some area of the lower section of the specimen of Fig. 2 under the PM, from which we can see more clearly the increase of domains upon heating. A new domain often appears abruptly as a wedge-shaped one and then becomes longer and longer until it runs through the whole specimen. It is interesting that, when T is raised above 100 °C, many microdomains emerge in the crystal and the domain boundaries repel one another. Thus, they form nearly periodic polydomain structures. The increase of temperature can reduce the periodicity. Meeks and Duld[14] have reported that periodic domain arrays can be generated by applying suitable shear forces at room temperature and they may have potential applications. Here we find the increase of temperature can also generate regular domain arrays and tune their periodicity. This periodic structure is one in which the free-energy cost of forming a domain boundary decreases with increasing temperature.

When T is close to T_c, numerous microdomains fill the crystal and they alter from one state to the other frequently, while some wide stripe domains usually remain unchanged. When the contrasts of the microdomains become weaker and weaker till they disappear at $T=T_c$, the wide ones do not disappear completely yet [Fig. 6(d)]. As the temperature is raised above T_c, the wide domains disappear gradually and the contrast of the specimen becomes homogeneous [Fig. 6(e)]. The wide domains are believed to be caused by heterogeneous stress or defect-induced domains, whose physical properties and the nature of the phase transition are influenced by the stress field in the specimen.

Upon cooling, domains are reintroduced in a reversal way: the wide stripe domains appear first, then do the microdomains. When the temperature becomes lower, microdomains disappear, as shown in Figs. 6(f)–6(g). No thermal hysteresis is found during this optical observation.

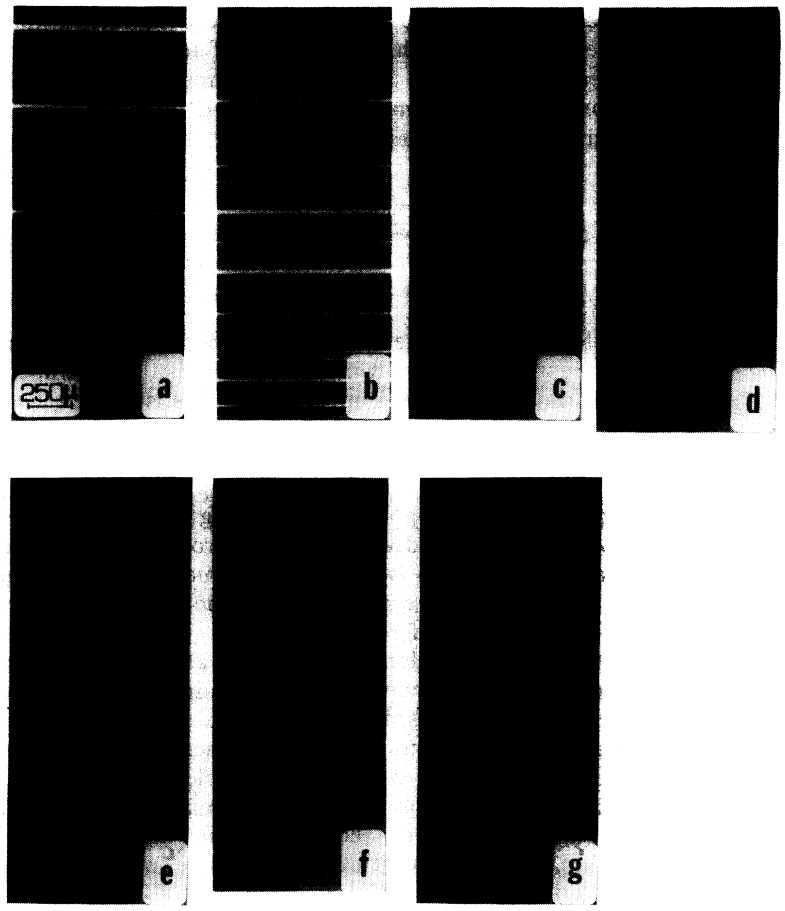

FIG. 6. Polarizing light observation of the phase transition of NPP. The temperatures from (a) to (g) are 20.0, 70.0, 139.0, 144.3, 149.0, 144.2, and 100.0°C, note the stress-preserved ferroelastic stripe at T_c.

V. DISCUSSION AND CONCLUSION

White-beam SR topography and PM observation bears evidence of ferroelasticity in NPP and the experimental results are well consistent with the classical Landau theory within our experimental precision. However, in most of our explanations, we do not account for the influence of mechanical stresses. In fact, mechanical stresses can greatly effect the ferroelasticity of NPP. First, NPP is much more sensitive to the stresses than other ferroelastics[13] and consequently the distribution of domains are mainly related to the existence of external or internal stress. External stress can reproducibily reverse a domain from one state to the other or maintain a single-domain structure.[10] Domains in a free NPP crystal are usually produced by internal stress although many other factors including defects can weakly influence the domain patterns. Figure 7 shows a polydomain structure trapped in the vicinity of the internal local stress field at room temperature. Second, mechanical stresses can also influence the phase transition. In Sec. IV we have found that some wide stripe domains in the vicinity of internal local stress field often do not disappear at T slightly above T_c, which indicates that stress may preserve ferroelastic phase above T_c. To fully understand the ferroelastic-paraelastic phase transition, we should take into account the coupling between the stress and the spontaneous strain, just like that in $SiTiO_3$.[4] For simplicity, if we assume that the coupling energy density between the stress field $\mathbf{h}$ and the spontaneous strain η takes the simplest form of $-\eta h$, then the free-energy density of the system is

$$\Phi_h(P,T,\eta)=\Phi_0(P,T)+A_0(T-T_c)\eta^2+B_0\eta^4-\eta h \ . \tag{21}$$

By minimizing Eq. (21) with respect to η, we obtain the equilibrium condition to be

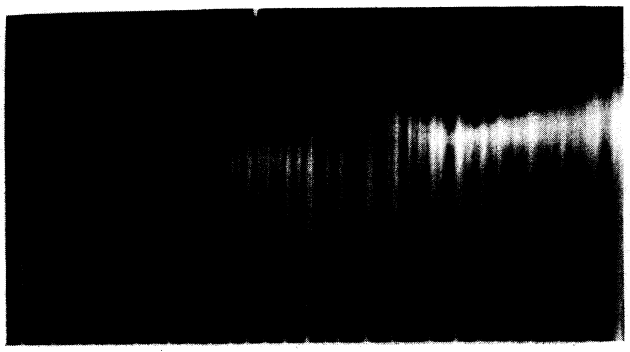

FIG. 7. Optical microphotograph showing internal local stress-induced domain arrays at $T=20.0$°C.

$$2A_0(T-T_c)\eta+4B_0\eta^3=h \ . \tag{22}$$

For $T>T_c$, the minimum of Φ_h takes at $\eta\neq 0$. This effect may result in the existence of some stress-preserved domains in the orthorhombic phase. In the topographs, we did not observe image displacement above T_c. It may be inferred that the spontaneous strain e_5 of the preserved domains above T_c is so small that it produces no detectable contrast or displacement in topographs. Most twin boundaries in a free NPP are *a*-type twins. The *b*-type twins usually emerge in some local stress field at high temperature. This indicates that the energy of a *b*-type boundary is much higher than that of an *a*-type boundary.

ACKNOWLEDGMENTS

This work was supported by the National Natural Science Foundation of China.

[1]Kêitsiro Aizu, J. Phys. Soc. Jpn. **27**, 387 (1969).
[2]L. F. Kirpichnikova, L. A. Shuvalov, A. A. Urusovskaya, N. R. Ivanov, and G. A. Kiosse, Ferroelectrics **140**, 1 (1993).
[3]C. Boulesteix, Phase Trans. **14**, 41 (1989).
[4]Wenwu Cao and James A. Krumhansl, Phys. Rev. B **42**, 4334 (1990).
[5]J. Y. Zhao, P. Yang, S. S. Jiang, X. M. Jiang, J. H. Jiang, D. C. Xian, Z. H. Geng, and Q. Zou, Appl. Phys. Lett. **59**, 1952 (1991).
[6]Z. W. Hu, S. S. Jiang, P. Q. Huang, X. R. Huang, D. Feng, J. Y. Wang, and L. X. Li, Appl. Phys. Lett. **64**, 55 (1994).
[7]G.-D. Yao, M. Dudley, Y. Wang, X. Liu, and R. C. Liebermann, Mater. Sci. Eng. A **132**, 23 (1991).
[8]S. S. Jiang, Z. W. Hu, P. Yang, and D. Feng, Ferroelectrics **140**, 71 (1993).
[9]Gilles Errandonea, Phys. Rev. B **21**, 5221 (1980).
[10]J. P. Budin, A. Milatos-Roufos, Nguyen Duc Chinh, and G. Le Roux, J. Appl. Phys. **46**, 2867 (1975).
[11]Michel Guymont, Phys. Rev. B **18**, 5385 (1978).
[12]J. Sapriel, Phys. Rev. B **11**, 5128 (1975).
[13]H. P. Weber, B. C. Tofield, and P. F. Liao, Phys. Rev. B **11**, 1152 (1975).
[14]S. W. Meeks and B. A. Duld, Appl. Phys. Lett. **47**, 102 (1985).

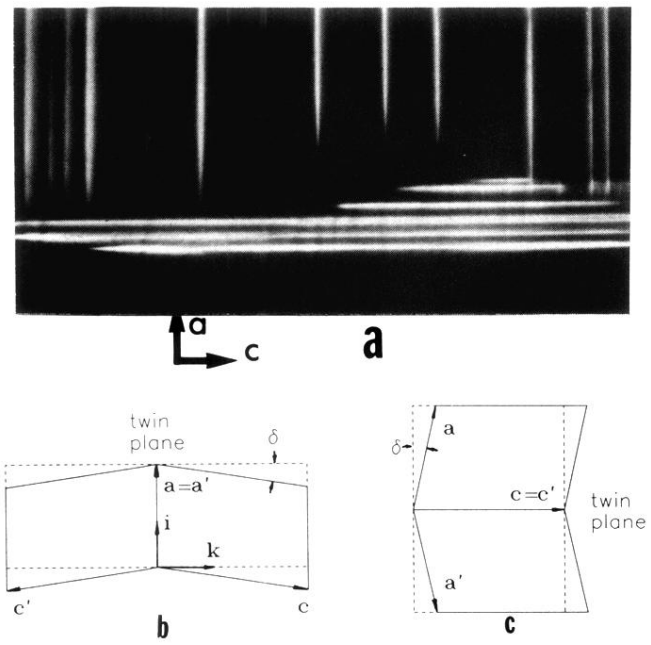

FIG. 1. Twinning in NPP. (a) Optical visualization of *a*-type twins (vertical domains) and *b*-type twins (horizontal domains); (b) *a*-type twin structure; (c) *b*-type twin structure.

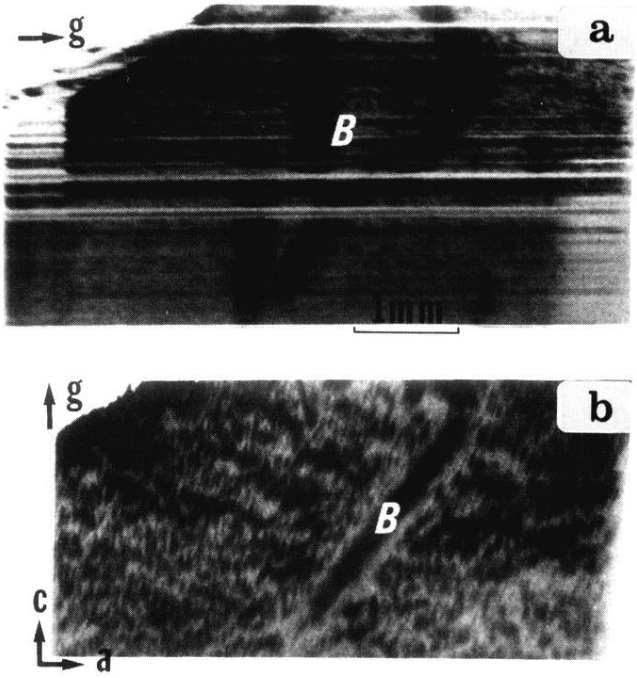

FIG. 2. SR topographs of NPP at room temperature; *B*, growth sector boundaries. (a) 200 reflection showing displacements of *a*-type twin images; (b) 001 reflection showing no contrast of twin.

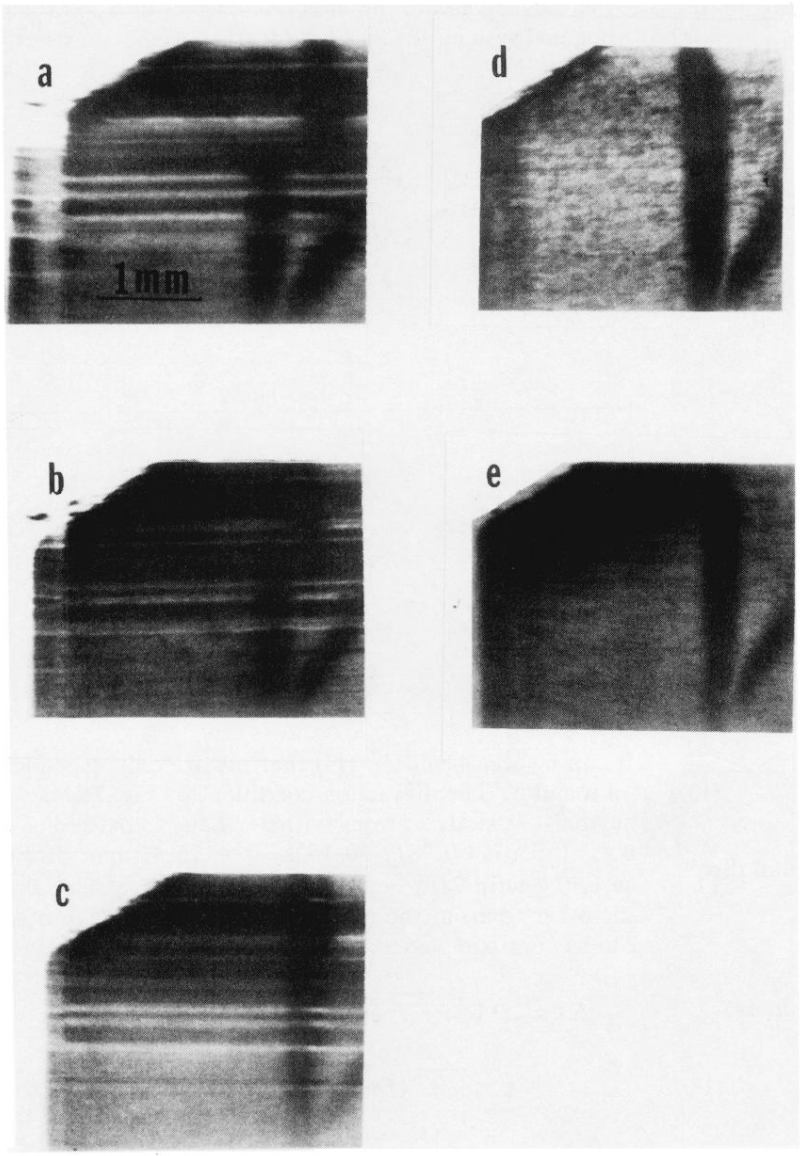

FIG. 4. 200 reflection topographs showing the phase transition of NPP. The temperatures from (a) to (e) are 85.0, 124.0, 140.0, 144.4, and 144.3 °C, respectively. In these figures the decrease of the image displacements is demonstrated. The black contrast to the upper-left section of (e) shows the phase instability.

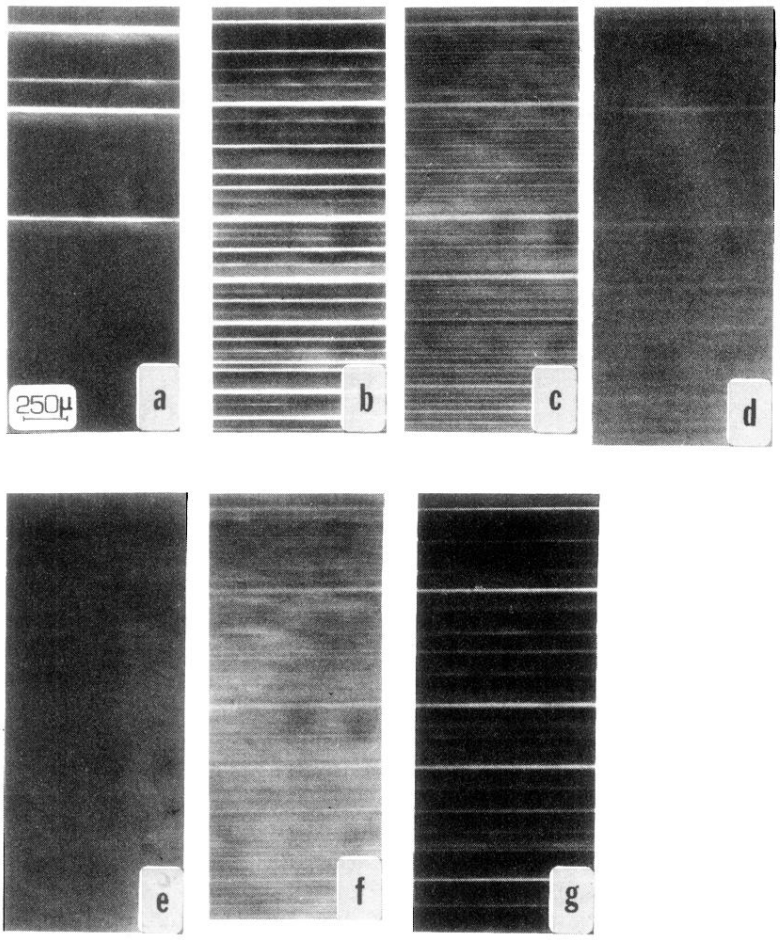

FIG. 6. Polarizing light observation of the phase transition of NPP. The temperatures from (a) to (g) are 20.0, 70.0, 139.0, 144.3, 149.0, 144.2, and 100.0°C, note the stress-preserved ferroelastic stripe at T_c.

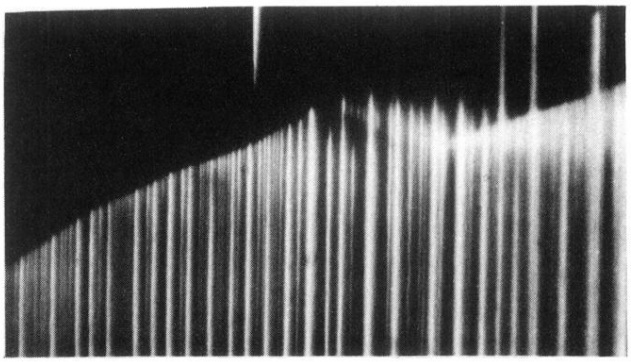

FIG. 7. Optical microphotograph showing internal local stress-induced domain arrays at $T = 20.0\,^{\circ}\mathrm{C}$.